


## Directional transport along an atomic chain

R. Gutiérrez-Jáuregui<sup>\*</sup> and A. Asenjo-García<sup>†</sup>

*Department of Physics, Columbia University, New York, New York 10027, USA*

 (Received 23 November 2021; accepted 9 March 2022; published 4 April 2022)

Motivated by a recent prediction to engineer the dispersion relation of a waveguide constructed from atomic components [Phys. Rev. Res. **4**, 013080 (2022)], we explore the possibility of creating directional transport in an open, collective quantum system. We characterize the optical response of this atomic waveguide through a scattering-matrix formalism built upon theories of photoelectric detection that allows us to find the conditions for directional mode-to-mode transmission to occur. We find that directional waveguides allow for an efficient outcoupling of light by reducing backscattering channels at the edges. This reduced backscattering is seen to play a major role in the dynamics when disorder is included numerically. A directional waveguide is shown to be more robust to localization, but at the cost of increased radiative losses.

DOI: [10.1103/PhysRevA.105.043703](https://doi.org/10.1103/PhysRevA.105.043703)

### I. INTRODUCTION

An excited atom in free space will eventually find a way to its ground state. In this spontaneous emission process, energy is originally localized inside a small volume from which it is set to travel outwards in the form of free photons [1,2]. When the atom is part of a dense and ordered atomic array, the excitation still finds a way out of the ensemble, but it does so through collective decay channels whose spatial and temporal profiles depend on the geometry of the array [3–8]. The most simple example is that of a one-dimensional (1D) chain where an excitation can travel without losses until it finds an edge to escape through. These atomic arrays provide a versatile platform to study the controlled scattering of light in open, collective quantum systems whose response can be engineered and probed in real time [9].

Such versatility can be used to generate directional transport along a 1D array by controlling individual atomic constituents. Directional transport—where transmission is allowed in one direction and blocked in the other—has been at the center of intense research motivated in part to understand the motion of biological systems [10–12]. Ratchet-type models predict that directional transport occurs when parity and time-reversal symmetry are violated in an otherwise unbiased source [13], and have been studied using elaborate atomic configurations where the internal degrees of freedom are used to generate periodic but asymmetric potentials to create directionality [14–16]. These predictions have been supported by experimental observations using colloidal particles [17], polystyrene spheres [15,18], and cold rubidium atoms [16].

While these experiments describe the transport of material particles guided by an electromagnetic potential, an analogy is found in photonic systems where light is guided by mat-

ter [19–22]. The motivation behind directional transport in these platforms is to generate robust optical systems where backscattering is inhibited [23,24]. Through this constrain one can reduce the coupling to parasitic channels and, for imperfect materials, the interferences that give rise to localization [25–28].

In this manuscript we present a systematic description of the transport of excitations along a directional atomic chain. We begin by reviewing an idealized model for an atomic chain whose optical response is engineered to display directionality and calculate the transmittance of excitations via a scattering matrix. This approach is suitable to describe photons entering an atomic chain through a particular channel before leaving in another. We then derive the conditions for directionality and explore how to retrieve excitations efficiently from a directional chain. To finish, we include the effect of imperfections that break the periodicity of the array and show that backscattering is suppressed even in the presence of disorder.

### II. BACKGROUND: ATOMIC CHAINS

We consider an atomic chain made of  $\mathcal{N}$  tightly trapped atoms separated a distance  $a$  from their nearest neighbors. Each atom is characterized by its position  $\mathbf{r}_n$  and is assumed to have a ground state  $|g\rangle$  and three excited states  $|e_s^n\rangle$  of angular momentum projections  $s = \{0, \pm\}$ . States  $|e_+^n\rangle$  and  $|e_-^n\rangle$  are connected by a Raman transition as sketched in Fig. 1, where one leg of the transition is driven by a laser beam of amplitude  $\Omega_+$  and phase  $ik_c z_n$  (dependent on the atomic position) while the other is driven by a counterpropagating beam with amplitude  $\Omega_-$  and phase  $-ik_c z_n$ . Both beams share the same frequency  $\omega_c = k_c c$  and are far detuned from the atomic transition by  $\Delta = \omega_0 - \omega_c$ . Their superposition defines a control field that distorts the atomic state.

Under this configuration—and moving to an interaction picture with free Hamiltonian  $\sum_{n,s} \hbar\omega_c |e_s^n\rangle\langle e_s^n|$ —an effective

<sup>\*</sup>r.gutierrez.jauregui@gmail.com

<sup>†</sup>ana.asenjo@columbia.edu

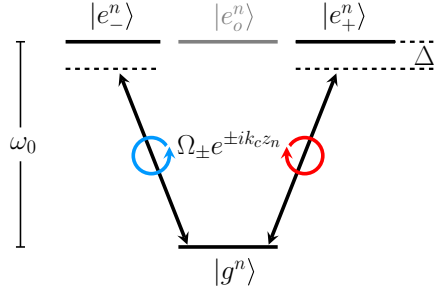


FIG. 1. Energy-level diagram to realize the effective Hamiltonian of Eq. (1) where two excited states, denoted by  $|e_+^n\rangle$  and  $|e_-^n\rangle$ , couple via a far-detuned Raman transition. Bold arrows represent the drive amplitudes  $\Omega_{\pm}$  generated by two counterpropagating beams of wave vector  $k_c$  and polarizations  $\epsilon_+$  and  $\epsilon_-$ , such that the phase acquired from this two-photon process depends on the atomic position  $z_n$ .

Hamiltonian for the  $n$ th atom is realized [9]:

$$\mathcal{H}^{(n)} = \sum_{s=\pm} \frac{\hbar}{2} (\Delta + \delta) (\sigma_{ss}^{(n)} - \sigma_{gg}^{(n)}) - \frac{\hbar\delta}{4} (1 - s \cos \theta) \sigma_{ss}^{(n)} + \frac{\hbar\delta}{4} \sin \theta (e^{-2ik_c z_n} \sigma_{+-}^{(n)} + e^{2ik_c z_n} \sigma_{-+}^{(n)}). \quad (1)$$

Here  $\sigma_{ss'}^{(n)} = |e_s^n\rangle\langle e_{s'}^n|$  is an operator connecting two atomic states;  $\delta = (\Omega_+^2 + \Omega_-^2)/2\Delta$  is the light shift induced by the beams; and  $\theta = 2 \arctan(\Omega_+/\Omega_-)$  is a mixing angle.

Atoms forming the chain interact with each other through the exchange of photons scattered in and out of the electromagnetic environment. In free space their dynamics can be understood in terms of an open quantum system by tracing out the state of the electromagnetic field under the Born and Markov approximations. The master equation for the collective state of the atomic chain  $\rho$  then reads

$$\dot{\rho} = \frac{1}{i\hbar} \left[ \sum_{n,m} \left( \mathcal{H}^{(n)} \delta_{nm} + \hbar \sum_{s,s'} \Delta_{ss'}^{nm} \sigma_{sg}^{(n)} \sigma_{gs'}^{(m)} \right), \rho \right] + \mathcal{L}[\rho], \quad (2)$$

where  $\mathcal{L}$  is the Lindblad superoperator,

$$\mathcal{L}[\bullet] = \sum_{n,m,s,s'} \frac{\gamma_{ss'}^{nm}}{2} (2\sigma_{gs}^{(n)} \bullet \sigma_{s'g}^{(m)} - \sigma_{s'g}^{(m)} \sigma_{gs}^{(n)} \bullet - \bullet \sigma_{s'g}^{(m)} \sigma_{gs}^{(n)}),$$

and the parameters  $\Delta_{ss'}^{nm}$ ,  $\gamma_{ss'}^{nm}$  represent the collective frequency shift and decay rate. These parameters depend on the relative position between two atoms  $n$  and  $m$  and their transition dipole moment through the free-space electromagnetic Green function [29].

This chain supports the lossless transport of excitations via collective subradiant states generated by destructive interference of individual radiation paths. Subradiant states appear below a limiting lattice constant [5],

$$a \leq \lambda_0/2 = \pi c/\omega_0, \quad (3)$$

and are characterized by vanishing eigenvalues of the collective decay matrix  $\gamma_{ss'}^{mn}$ . As we show below, the subradiant channels can be engineered to be directional by changing the parameters of the effective Hamiltonian of Eq. (1). This is a consequence of the control field that deforms the atomic

dipole moment—first by creating an asymmetric frequency shift that breaks the degeneracy between  $|e_{\pm}^n\rangle$  states as an effective magnetic field would, and second by orienting the dipole moment in a spatially dependent way, thus changing the way each atom probes the local environment and its coupling to neighboring sites.

### III. SCATTERING MATRIX FORMALISM

Previous research on the transport through atomic arrays has been focused on the flux of excitations from one end of the chain to the other. Yet, when it comes to describing the light that enters and leaves the array, standard studies rely on physical intuition [30,31] or additional boundary conditions [32–35] that restrict the coupling to the edges of the array. This has proved to be a powerful tool to describe collective atomic systems, but overlooks the spatial and temporal profiles of the input and output fields that are ultimately measured in an experiment and can be problematic when discussing the mode-to-mode transmissions required for directional transport [21].

We develop here a scattering approach that describes the transport of excitations along an atomic chain. This method captures the absorption of a traveling photon by the chain and its ensuing emission into a desired channel. The method is built from the theory of photoelectric detection [36] and calculations for the scattering amplitudes of a photon by atomic systems [37]. In contrast to the master equation shown above, our focus now lies on free electromagnetic fields that, once detected, can be used to infer the emission path followed.

To find the scattering matrix we take a step back and consider a system composed of the chain and its surrounding electromagnetic environment. These are described, respectively, by free Hamiltonians:

$$\mathcal{H}_S = \sum_n \mathcal{H}^{(n)}, \quad (4)$$

$$\mathcal{H}_R = \sum_{k,\lambda} \hbar \omega_k b_{\mathbf{k},\lambda}^\dagger b_{\mathbf{k},\lambda}, \quad (5)$$

where  $b_{\mathbf{k},\lambda}$  is the annihilation operator for a free electromagnetic mode of wave vector  $\mathbf{k}$ , frequency  $\omega_k$ , and polarization  $\epsilon_{\mathbf{k},\lambda}$ . The subsystems couple through a dipolar term,

$$\mathcal{H}_{SR} = \hbar \sum_{k,\lambda} \sum_{n,s} \kappa_{\mathbf{k},\lambda}^{n,s} b_{\mathbf{k},\lambda}^\dagger \sigma_{gs}^{(n)} + \kappa_{\mathbf{k},\lambda}^{n,s*} b_{\mathbf{k},\lambda} \sigma_{sg}^{(n)}, \quad (6)$$

whose coupling parameter,

$$\kappa_{\mathbf{k},\lambda}^{n,s} = \sqrt{\frac{\omega_k}{2\hbar\epsilon_0\mathcal{V}}} e^{-i\mathbf{k}\cdot\mathbf{r}_n} \epsilon_{\mathbf{k},\lambda} \cdot \mathbf{d}_s^{(n)}, \quad (7)$$

illustrates how atoms probe the local amplitude of the electric field through their dipole moment  $\mathbf{d}_s$ . For convenience we have considered a quantization volume  $\mathcal{V}$  for the electromagnetic modes that will later be taken to infinity.

The free electric field operator is obtained by solving the Heisenberg equations of motion for the complete Hamiltonian  $\mathcal{H} = \mathcal{H}_S + \mathcal{H}_R + \mathcal{H}_{SR}$  under the Born and Markov approximations. The resulting field separates into free and scattered fields [37–39]:

$$\mathbf{E}(\mathbf{R}, t) = \mathbf{E}_{\text{free}}(\mathbf{R}, t) + \mathbf{E}_{\text{scatt}}(\mathbf{R}, t), \quad (8)$$

where the positive frequency component of the latter is given in the far field by

$$\mathbf{E}_{\text{scatt}}^{(+)}(\mathbf{R}, t) = \sqrt{\frac{\hbar\omega_0}{2\epsilon_0 c}} \frac{3\Gamma_0}{8\pi} \sum_{n,s} \frac{[1 - (\mathbf{d}_s \cdot \mathbf{R}_n)^2]^{1/2}}{R_n} \hat{\epsilon}_{ns} \times e^{-i r_n k_0} \sigma_{gs}^{(n)}(t - R/c). \quad (9)$$

Here  $\mathbf{R}_n = \mathbf{R} - \mathbf{r}_n$  is the distance between the  $n$ th atom and a point where the field is probed, while  $\hat{\epsilon}_{ns}$  is a unitary vector pointing in the direction  $\mathbf{R}_n \times (\mathbf{R}_n \times \mathbf{d}_s)$  that accounts for the radiation profile of each atom with an individual decay rate,

$$\Gamma_0 = \frac{1}{4\pi\epsilon_0} \frac{4\omega_0^3 |d_s|^2}{3\hbar c^3}. \quad (10)$$

The scattered field can be used to probe the state of the atomic chain using Eq. (9). Consider then a set of photodetectors surrounding the atomic chain that record all the photons being scattered into the environment. These detectors are placed at the positions  $\mathbf{R}_{\theta\phi} = (R, \theta, \phi)$ , with each one covering a surface area  $R^2 \Delta\Omega$  of solid angle  $\Delta\Omega$  and considered capable of resolving the polarization state  $\hat{\epsilon}_\lambda$  and arrival time of the photons. The information gained after each detection can be traced back to the state of the chain by applying the jump operator,

$$\mathcal{J}_{\theta\phi\lambda} = \sqrt{\frac{2\epsilon_0 c}{\hbar\omega_0}} (R^2 \Delta\Omega) \mathbf{E}_{\text{scatt}}^{(+)}(\mathbf{R}_{\theta\phi}) \cdot \hat{\epsilon}_\lambda, \quad (11)$$

and accounting for the necessary free evolution. These operators have units of square root of photon flux, such that

$$P_{\theta\phi\lambda} = \tau \text{Tr}_S[\mathcal{J}_{\theta\phi\lambda} \rho \mathcal{J}_{\theta\phi\lambda}^\dagger] \quad (12)$$

gives the probability for a chain in state  $\rho$  to scatter into the detector  $(\mathbf{R}_{\theta\phi}, \hat{\epsilon}_\lambda)$  during a small time interval  $\tau$ . The trace is taken over atomic variables only.

Equations (9)–(12) give the basic tools to unravel the state of the atomic chain subject to a particular measurement record and recover the path an excitation followed across the chain [36]. We, however, are not interested in the particular times at which an input photon enters and an output photon leaves an otherwise empty chain; but we are interested in the probability amplitude for the process to take place. A sum over all the records where this process took place is given by the scattering  $\mathcal{S}$  matrix whose components  $S_{ba} = \langle g; b | \mathcal{S} | g; a \rangle$  give the probability amplitude for a free field of energy  $E_a$  and state  $|a\rangle$  (e.g.,  $|\mathbf{k}_a, \lambda_a\rangle$ ) to scatter into one of energy  $E_b$  and state  $|b\rangle$ . In the reciprocal space these components are written as [37]

$$S_{ba}(E_a) = \delta_{\lambda_a, \lambda_b} \delta(\mathbf{k}_a - \mathbf{k}_b) - 2\pi i \delta(E_a - E_b) \mathbf{T}_{ba}, \quad (13)$$

with

$$\mathbf{T}_{ba} = \sum_{ns, ms'} \langle g; 0 | (\hbar\kappa_{\mathbf{k}_b, \lambda_b}^{n, s*} \sigma_{gs}^{(n)}) \mathcal{Q} \frac{1}{E_a - \tilde{\mathcal{H}}} \mathcal{Q} (\hbar\kappa_{\mathbf{k}_a, \lambda_a}^{m, s'} \sigma_{gs}^{(m)}) | g; 0 \rangle. \quad (14)$$

This transmission matrix  $\mathbf{T}$  divides environment and chain by connecting free fields to spin waves through the operator  $\mathcal{Q} = \sum_{n,s} |e_s^n; 0\rangle \langle e_s^n; 0|$ , a projector into the subspace where one excitation populates the chain and the field is in the vacuum

state. Once in this subspace, the resolvent  $G(E) = (E - \tilde{\mathcal{H}})^{-1}$  determines the channels the excitation can follow. This is done through a non-Hermitian Hamiltonian,

$$\tilde{\mathcal{H}} = \mathcal{H}_S - \sum_{n,m=1}^N \sum_{s=\pm} \hbar(\Delta_{ss}^{nm} + i\gamma_{ss}^{nm}) \hat{\sigma}_{sg}^{(n)} \hat{\sigma}_{gs}^{(m)}, \quad (15)$$

that acts over atomic states only and displays the collective frequency shifts and decay rates caused by their self-consistent interaction with the environment [in connection to the master equation of Eq. (2)].

We now bring together the picture provided by the jump operators of Eq. (11) and the  $\mathcal{S}$  matrix of Eq. (13) to study the transport along the chain. The key point is that the atomic ensemble only responds to free-field modes whose frequencies are close to the atomic resonance frequency  $\omega_0$ . For these frequencies, we can write [38]

$$\sum_{ns} \kappa_{\mathbf{k}_b, \lambda_b}^{ns*} \sigma_{gs}^{(n)} = \frac{1}{\sqrt{2\pi g(\omega_0)}} \mathcal{J}_{p_b q_b \lambda_b}, \quad (16)$$

where  $g(\omega_0) = R_V / 6\pi c$  is the optical mode density at the atomic transition frequency. Thus, after integrating Eq. (13) over a small range of output modes  $(N, N + dN)$  with  $dN = g(\omega_0) d\omega_b$ , the  $\mathcal{S}$  matrix takes the form,

$$\mathcal{S}(E) = \mathbb{1} - i\mathbf{t}(E), \quad (17)$$

where  $\mathbb{1}$  is the identity matrix and the transmission matrix,

$$\mathbf{t}(E) = \left( \sum_{\beta} \mathcal{J}_{\beta} \right) \frac{1}{E - \tilde{\mathcal{H}}} \left( \sum_{\alpha} \mathcal{J}_{\alpha}^{\dagger} \right), \quad (18)$$

accounts for all input and output modes through a sum of jump operators  $\mathcal{J}_{\beta}, \mathcal{J}_{\alpha}^{\dagger}$  that runs over all detectors  $(\theta, \phi, \lambda)$ . This transmission determines the channels through which a photon enters the chain, propagates across it, and then scatters out.

Equations (17) and (18) describe the main result of this section. They present a contextual description for the transport of excitations where input and output channels are given by the jump operators  $\mathcal{J}_{\theta\phi\lambda}^{\dagger}$  and  $\mathcal{J}_{\theta\phi\lambda}$ . And, while developed with a scattering picture in mind, these equations can be written in a form that is more suitable for transport by choosing a different set of jump operators. We could choose, for example, the jump operators given by the eigenvectors of the collective decay matrix  $\gamma_{ss}^{nm}$  denoted here by  $|\phi^{(v)}\rangle = \sum c_{ns}^{(v)} |e_s^n\rangle$  with eigenvalues  $\gamma_v$ . Under this unraveling the jump operators take the form,

$$\mathcal{J}_v = \sqrt{\gamma_v} \sum_{n,s} c_{ns}^{(v)} \sigma_{gs}^{(n)}. \quad (19)$$

The normal mode representation written in Eq. (19) and the physical space representation of Eq. (11) are connected through the equality,

$$\sum_{n,m,s} \gamma_{ss}^{nm} \sigma_{gs}^{(n)} \cdot \sigma_{sg}^{(m)} = \sum_{\alpha} \mathcal{J}_{\alpha} \cdot \mathcal{J}_{\alpha}^{\dagger}, \quad (20)$$

where  $\alpha$  runs along  $\{v\}$  or  $\{\theta, \phi, \lambda\}$  to select a representation. For  $\alpha = \{\theta, \phi, \lambda\}$  the right-hand side describes fields measured at particular points while for  $\alpha = v$  it focuses on fields radiated by the normal modes, which have only a formal meaning. Notice that both sets of jump operators guarantee a

unitary  $\mathcal{S}$  matrix since

$$\tilde{\mathcal{H}} - \tilde{\mathcal{H}}^\dagger = \sum_{\alpha} \mathcal{J}_{\alpha}^\dagger \mathcal{J}_{\alpha}. \quad (21)$$

A similar formula for the  $\mathcal{S}$  matrix has been used to study nuclear reactions [41,42] and has also emerged in the context of mesoscopic systems [30,31] where focus is placed on the resonance spectra and its relation to its transport properties [43] rather than on the connection to scattering records.

#### IV. TRANSPORT IN DIRECTIONAL CHAINS

The scattering matrix is now used to analyze the transmission across an atomic chain with emphasis on its directionality. This is done by considering the system Hamiltonian of Eq. (4) and the normal mode representation of Eq. (19) (jump operators with  $\alpha = \nu$ ). We begin by shifting our attention from the scattered field towards the atomic states using the components  $\mathcal{S}_{ns;ms'}$  of Eq. (17), which represent the probability amplitude for a photon to enter the chain through the individual atomic state  $|e_s^m\rangle$  and leave through  $|e_s^n\rangle$  disregarding the photonic spatial profile.

An optical medium presents directionality when the propagation of excitations along two opposing paths displays different mode-to-mode transmissions [21]. This occurs when reciprocity is broken, a condition that is represented by an asymmetric scattering matrix such that

$$\mathcal{S}_{ns;ms'}(E) \neq \mathcal{S}_{ms';ns}(E). \quad (22)$$

For the atomic chain described above, reciprocity is broken when collective decay and free operators do not commute:

$$\left[ \mathcal{H}_S, \sum_{n,m=1}^{\mathcal{N}} \sum_{s=-1}^1 \gamma_{ss}^{nm} \sigma_{sg}^{(n)} \sigma_{gs}^{(m)} \right] \neq 0. \quad (23)$$

This condition is satisfied for  $\theta \neq n\pi$  and  $\omega_c z_n / c \neq n\pi/2$  for all  $n$ . The first requirement leads to an asymmetric frequency shift of  $|e_+^n\rangle$  and  $|e_-^n\rangle$  states, an effective Zeeman shift created from the atomic response to the elliptic polarization of the control field. The second requirement corresponds to a subwavelength rotation of the atomic dipoles that is generated from the polarization gradient of the same field. These two requirements—simultaneous time-reversal and parity symmetry breaking—were found to be necessary for a waveguide made from plasmonic particles to break reciprocity and display directionality [19]. Equation (23) formalizes this result and extends it for an atomic chain.

Figure 2 shows the transmittance as a function of the input photon frequency for a chain of  $\mathcal{N} = 205$  atoms under conditions of reciprocity in Fig. 2(a) and nonreciprocity in Fig. 2(b). The transmittance is given by  $\sum_{s,s'} |\langle n, s | \mathcal{S} | m, s' \rangle|^2$  with  $n = 1$  (or  $\mathcal{N}$ ) and  $m = \mathcal{N}$  (1), which gives the probability for a photon to be absorbed by an atom at one end of the chain and be emitted at the opposite end. The transmittance for right- and left-propagating excitations, plotted as green and blue lines, respectively, displays an imbalance when reciprocity is broken. In both cases transmission channels appear as narrow resonances due to the atom-atom interactions [40]. As more atoms are added to the chain, additional resonances with a narrowing width begin to appear, thus opening a broad trans-

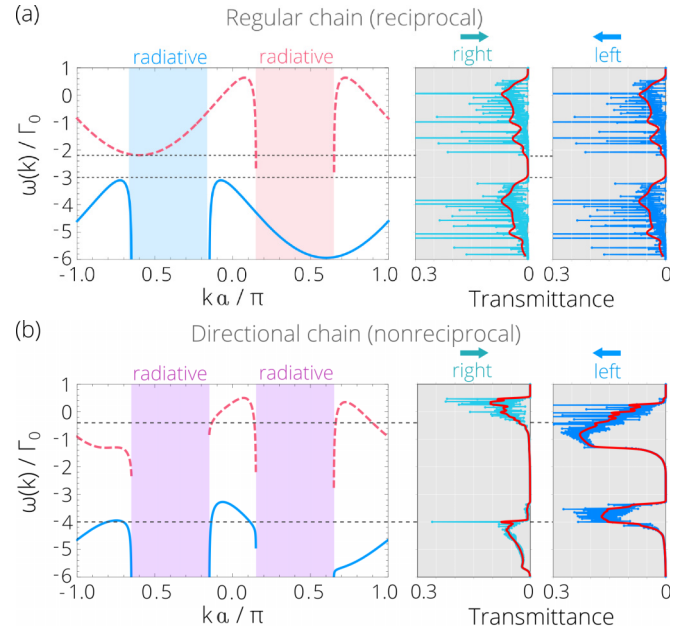


FIG. 2. Dispersion relation for an infinite chain and transmittance of a finite chain of  $\mathcal{N} = 205$  atoms under conditions of regular and directional transport. The transmittance is obtained from  $\sum_{s,s'} |\langle n, s | \mathcal{S} | m, s' \rangle|^2$  [see Eq. (17)] with  $n, m$  denoting the emission from atoms at the end of the chain. The dispersion displays two transparency windows given by the frequencies of  $|u, k\rangle$  (dashed pink) and  $|l, k\rangle$  (solid blue) subradiant states of Eq. (24). A nonzero transmittance is found for incoming photons whose energies match the narrow resonances of the subradiant modes that fill the transparency window, as shown by gray dashed lines. Red lines in the transmittance indicate the average over a small energy interval to visualize the infinite chain limit. For both plots the lattice constant is  $a = \lambda_0/8$  and the Raman channels of Eq. (1) have a strength  $\delta = 10\Gamma_0/3$  and phase  $k_c = \pi/5a$  with  $\theta = 0$  in (a) and  $\theta = \pi/4$  in (b).

parency window where an excitation can propagate without losses. We have considered atoms at the edges since subradiant channels tend to scatter out of the chain at these points. While not shown in the figure, the transmittance is reduced for atoms  $n, m$  separated from the edge as they are more likely to absorb photons through short-lived superradiant channels.

We also plot the dispersion relation of the atomic chain in Fig. 2. The dispersion marks the location and frequency spread of the subradiant states. It is obtained in the infinite chain limit by diagonalizing the non-Hermitian Hamiltonian (15) as done in Ref. [9]. In this limit subradiant states are determined by a wave vector  $k$  directed along the chain axis and a polarization index  $\{u, l\}$ . Written within the free basis these states read

$$|u, k\rangle = \sum_n e^{ikz_n} \sum_{s=\pm} [e^{-iskc z_n} c_{u,s}^{(n)} \hat{\sigma}_{sg}^{(n)}] |g\rangle^{\otimes \mathcal{N}}, \quad (24a)$$

$$|l, k\rangle = \sum_n e^{ikz_n} \sum_{s=\pm} [e^{-iskc z_n} c_{l,s}^{(n)} \hat{\sigma}_{sg}^{(n)}] |g\rangle^{\otimes \mathcal{N}}, \quad (24b)$$

where the local phase  $k_c z_n$  is inherited from the Raman transition sketched in Fig. 1 and the probability amplitudes  $c_{u/l,s}^{(n)}$  take a simple form given in Ref. [9]. The dispersion relations

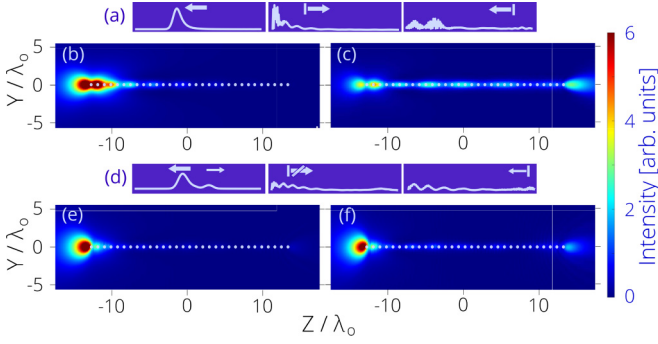


FIG. 3. Backscattering from a spin wave bouncing off the ends of a chain under conditions for regular (a)–(c) and directional transport (d)–(f) used in Fig. 2. Panels (a) and (d) represent the atomic population before (left) and after the first (center) and second bounces (right). Notice the interference that arises in the central panel of the regular chain and is missing in the directional chain. Through Eq. (25) we have decided to excite two different-frequency modes of the directional chain to exemplify how the backscattering is completely suppressed for the left-propagating mode while reduced for the right-propagating one. The scattered field intensity at first [(b) and (e)] and second [(c) and (f)] bounces shows the imbalance in left and right transmissions of a directional chain that can be used to route light efficiently.

of these two branches are drawn in Fig. 2 as dashed pink lines for the upper  $u$  branch and solid blue lines for the lower  $l$  branch. Subradiant states are shown to appear for quasimomentum lying beyond the light line  $|k \pm k_c| > \omega_0/c$ , where radiation paths between different atoms can interfere destructively and cancel out the collective radiation, and create a transparency window whose width scales with the atomic separation  $a$  as  $\sim \Gamma_0/(k_0 a)^3$ . As shown in Fig. 2 the transparency window obtained by the scattering matrix method coincides with that generated by the dispersion relation of the subradiant states. Subradiant states can then be understood as guided modes that propagate along the chain without scattering.

The dispersion relation also provides a geometrical picture for the density of states of the chain and, through its derivative, the group velocities of traveling spin waves. When reciprocity is satisfied, the dispersion is symmetrical and the chain displays two counterpropagating channels for each frequency. When reciprocity is broken, the dispersion relation becomes asymmetrical and counterpropagating channels display different transmittances.

#### A. Emission from a traveling spin wave

The radiation paths are not canceled completely for finite arrays, thus coupling subradiant modes to the environment and to each other. The backscattering into other modes, however, can be inhibited for directional chains and light can be routed into a given direction. This is exemplified in Fig. 3 where we plot the intensity of a field scattered by a spin-wave traveling inside the chain under conditions of regular and directional transport. We illustrate the different behaviors by considering a single-excitation initial state,

$$|\psi\rangle = c_g |g\rangle^{\otimes N} + c_e \sum_n \frac{a}{\sqrt{2\pi} \Delta x} e^{ia(k+k_c) - \frac{a^2(n-n_0)}{\Delta x^2}} |e_n^-\rangle, \quad (25)$$

that is set to evolve under the non-Hermitian Hamiltonian of Eq. (15). The chain is weakly populated ( $|c_e|^2 = 0.2$ ) and the excitation is centered around the site  $n_0 = 100$  with spatial width  $\Delta x^2 = 60a^2$  and central quasimomentum  $k = 0$ . The evolution of this spin wave is sketched in Figs. 3(a) and 3(d) where the atomic population is plotted at three different times: (i) before the wave reaches the end of the chain, (ii) as it reaches this end and is backscattered, and (iii) as the backscattered wave reaches the opposite end. The scattered field intensity at times (ii) and (iii) is plotted, respectively, in Figs. 3(b) and 3(c) for the regular chain and in Figs. 3(e) and 3(f) for the directional chain, following Eq. (9). In both cases the intensity of the field is concentrated at one end of the chain as the spin wave is bounced off the edge [Figs. 3(b) and 3(e)], but, with imbalanced backscattering channels, the ensuing spreads vary significantly [Figs. 3(c) and 3(f)]. A spin-wave bouncing off one end of a regular chain backscatters into several subradiant channels that guide it to the opposite end. This is suggested by the scattered field intensity and the interference profile in the atomic population. In a directional chain, by contrast, the spin wave has fewer channels to backscatter into and the emission remains localized off one end, as suggested by the population profile. The scattered field remains trapped on one edge, radiating efficiently into one direction and causing for the interference pattern in the atomic population to vanish.

Figures 3(d)–3(f) show two different spin waves propagating along the directional chain. These counterpropagating waves result from the initial state of Eq. (25) that overlaps with both excitation branches since the Raman channels responsible for the directional response couple  $|e_n^-\rangle$  and  $|e_n^+\rangle$  states. The response of each wave helps to illustrate the difference when backscattering channels are inhibited or completely absent. In the case of the  $u$  branch the spin wave can find states to backscatter, thus leading to a low-intensity field traveling along the chain and a reduced interference pattern on the atomic population. Both these properties are reduced for the  $l$  branch.

While we have attributed the imbalance between right- and left-propagating channels to the density of subradiant states, alternative methods can be used to quantify this behavior. For instance, in arrays of plasmonic particles, it was shown recently that the coupling between an excitation and a directional array can be exponentially weaker in one direction than in the other [44]. This was shown through a detailed study of the analytical properties of the Green function of the chain. Ultimately, both the Green function method of Ref. [44] and the eigenstates of Eq. (24) describe the propagation of single excitations inside arrays, but are traditionally used in different frameworks and regimes. Their close connection (compare, e.g., the structure of Eq. (7) of Ref. [9] and Eq. (24) of Ref. [44]) suggests that results found in classical optical systems can be explored in atomic arrays, such as conditions for nonreciprocity beyond one-dimensional chains [45].

#### V. EFFECT OF DISORDER

Throughout the last two sections we have connected the dynamics inside an atomic chain to the scattered field with the goal of studying the transport properties of a directional chain

and their relation to the far fields measured in an experimental setting. We have emphasized the role of subradiant states that guide an excitation from one end of the chain towards the other through lossless collective channels. With subradiant states emerging from the phase coherence between individual atomic constituents, the question remains as to how the transport of excitations is affected by imperfections of the array.

Imperfections can manifest in our model through individual frequency shifts caused by the trapping potential or displacements in the atomic positions due to weaker traps. The effect in both cases is to break the periodicity of the array. We introduce these imperfections below and compare the response between reciprocal and nonreciprocal chains, showing that the transport properties of the latter are more resilient to disorder.

We focus on individual frequency shifts for simplicity. They are given by an additional potential,

$$V = \sum_{n,s} \mathcal{E}_n \sigma_{ss}^{(n)}, \quad (26)$$

where  $\mathcal{E}_n$  is a stochastic variable distributed over a frequency band of zero mean and variance  $\sqrt{W}$ ,

$$\langle \mathcal{E}_n \rangle_{\text{avg}} = 0; \quad \langle \mathcal{E}_n \mathcal{E}_m \rangle_{\text{avg}} = W \delta_{nm}. \quad (27)$$

Since we are interested in the effect on the atomic coherence it is convenient to write this potential in the reciprocal space where

$$V = \sum_{n,s} \sum_{k,k'} \mathcal{E}_n e^{i(k-k')z_n} |e_s, k\rangle \langle e_s, k'|, \quad (28)$$

as obtained from the relation  $\langle k | e_s^{(n)} \rangle = e^{ikz_n} |e_s\rangle$ . A similar decomposition can be done for random atomic positions with the added complexity that the interaction strength can diverge for small lattice sites.

The role of this imperfection is to couple states of different quasimomentum  $k$ , causing a state of well-defined wave vector, e.g., a spin wave or a normal mode, to spread in reciprocal space and localize in position. For weak energy shifts whose variance is significantly smaller than the transparency window, the impurities can be treated as a stochastic disorder that deform the dispersion relation by coupling states of approximately the same energy. Ultimately, this coupling reduces the atomic coherence with a more pronounced effect over frequencies with a high density of states [28].

Due to the asymmetry in the dispersion relation of a nonreciprocal chain (see Fig. 2) a state of well-defined wave vector finds fewer modes to backscatter to than one inside the reciprocal chain, thus reducing the momentum spread. This is exemplified in Fig. 4 where we plot the population of a spin wave propagating inside an atomic chain for different disorder strengths and compare reciprocal and nonreciprocal responses. The spin wave is again prepared in the state (25). The plots show the distribution in position and reciprocal spaces after a time  $t = 13\Gamma_0^{-1}$  has passed with pink and blue lines used, respectively, for  $|e_+\rangle$  and  $|e_-\rangle$  polarizations. Notice first that when reciprocity is broken the superposition of the two excitation branches manifests as a beating in the

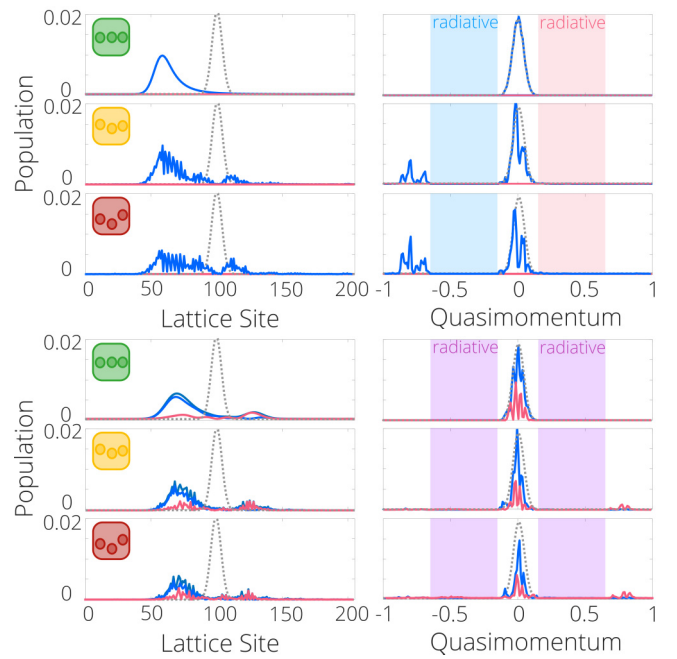


FIG. 4. Transport of a spin wave in the presence of disorder for the regular and directional chains of Fig. 2. Dashed gray lines denote the initial distribution while solid pink (blue) lines the population of  $|e_{+(-)}\rangle$  states after a time  $t = 13\Gamma_0^{-1}$  has passed. The populations oscillate with a frequency given by the energy difference between upper and lower branches and signal the excitation of two modes. Backscattering is completely inhibited for the blue mode. As the disorder strength is increased from  $\sqrt{W}/\Gamma_0 = 0, 0.625, 1.0$  between top and bottom panels, the collective state of the regular chain loses coherence while that of the directional chain preserves it. The disorder strengths are to be compared with the transparency window of  $2.5\Gamma_0$ .

population of  $|e_{\pm}\rangle$  states, readily seen in reciprocal space. The beating frequency corresponds to the energy separation between  $u$  and  $l$  branches. As the disorder strength is increased in Figs. 4(b) and 4(c) the state begins to scatter into different quasimomentum components. In the reciprocal case the spread begins to occupy all the available states while in the nonreciprocal case there is only a small spread over the upper branch  $|u\rangle$  where few modes are available. There is virtually no spread for the lower branch  $|l\rangle$  as there are no modes available.

The back and forward scattering eventually leads to localization of the excitation that prevents its transport [26]. For an atomic chain this localization describes a transient behavior: An excitation will eventually scatter out of the system through individual or collective channels. While the nonreciprocal chain has shown a reduced spread in momentum it arrives at the cost of a doubled radiation zone. It is found that, for the slow modes considered here, the loss is higher in the nonreciprocal case. This effect can be reduced for chains with a smaller lattice constant.

## VI. CONCLUSIONS

In summary, we have presented a method to generate and probe the directional transport of excitations along an atomic

chain. Directionality is achieved through an external control field that breaks the degeneracy between two excited states and induces a locally varying dipole moment that follows a helical pattern, thus breaking time-reversal and parity symmetries. We find a simple formula where the probability for a free photon to enter the chain, propagate along collective decay channels, and then scatter out is readily calculated. This approach is based on detected events and has a direct connection to methods developed for electron transport in condensed matter physics [46]. We show that defect-induced backscattering is suppressed in directional chains, and the phase coherence

between atoms of the chain survived for stronger disorder in comparison to regular chains. This, however, comes at the cost of increased decay rate for strong disorder due to the open nature of the system.

### ACKNOWLEDGMENTS

We thank A. Ortega and S. Cardenas-Lopez for insightful discussions. R.G.-J. and A.A.-G. acknowledge financial support by the National Science Foundation QII-TAQs (Grant No. 1936359), and CAREER (Grant No. 2047380).

- [1] M. Fischer, B. Srivathsan, L. Alber, M. Weber, M. Sondermann, and G. Leuchs, *Appl. Phys. B* **123**, 48 (2017).
- [2] R. Gutiérrez-Jáuregui and R. Jáuregui, *Sci. Rep.* **10**, 17383 (2020).
- [3] R. J. Bettles, S. A. Gardiner, and C. S. Adams, *Phys. Rev. Lett.* **116**, 103602 (2016).
- [4] G. Facchinetti, S. D. Jenkins, and J. Ruostekoski, *Phys. Rev. Lett.* **117**, 243601 (2016).
- [5] A. Asenjo-Garcia, M. Moreno-Cardoner, A. Albrecht, H. J. Kimble, and D. E. Chang, *Phys. Rev. X* **7**, 031024 (2017).
- [6] E. Shahmoon, D. S. Wild, M. D. Lukin, and S. F. Yelin, *Phys. Rev. Lett.* **118**, 113601 (2017).
- [7] S.-M. Yoo and J. Javanainen, *Opt. Express* **28**, 9764 (2020).
- [8] J. Rui, D. Wei, A. Rubio-Abadal, S. Hollerith, J. Zeiher, D. M. Stamper-Kurn, C. Gross, and I. Bloch, *Nature (London)* **583**, 369 (2020).
- [9] R. Gutiérrez-Jáuregui and A. Asenjo-Garcia, *Phys. Rev. Res.* **4**, 013080 (2022).
- [10] J. L. Mateos, *Phys. Rev. Lett.* **84**, 258 (2000).
- [11] D. Astumian and P. Hänggi, *Phys. Today* **55**, 33 (2002).
- [12] P. Hänggi and F. Marchesoni, *Rev. Mod. Phys.* **81**, 387 (2009).
- [13] P. Curie, *J. Phys. Theor. Appl.* **3**, 393 (1894).
- [14] J. Prost, J.-F. Chauwin, L. Peliti, and A. Ajdari, *Phys. Rev. Lett.* **72**, 2652 (1994).
- [15] J. Rousselet, L. Salome, and A. Ajdari, and J. Prost, *Nature (London)* **370**, 446 (1994).
- [16] C. Mennerat-Robilliard, D. Lucas, S. Guibal, J. Tabosa, C. Jurczak, and J.-Y. Courtois, and G. Grynberg, *Phys. Rev. Lett.* **82**, 851 (1999).
- [17] L. P. Faucheux, L. S. Bourdieu, P. D. Kaplan, and A. J. Libchaber, *Phys. Rev. Lett.* **74**, 1504 (1995).
- [18] A. V. Arzola, M. Villasante-Barahona, K. Volke-Sepúlveda, P. Jákl, and P. Zemánek, *Phys. Rev. Lett.* **118**, 138002 (2017).
- [19] Y. Hadad and B. Z. Steinberg, *Phys. Rev. Lett.* **105**, 233904 (2010).
- [20] Y. Hadad and B. Z. Steinberg, *Opt. Express* **21**, A77 (2013).
- [21] D. Jalas, A. Petrov, M. Eich *et al.*, *Nat. Photon.* **7**, 579 (2013).
- [22] D. L. Sounas and A. Alù, *Nat. Photon.* **11**, 774 (2017).
- [23] F. C. MacKintosh and S. John, *Phys. Rev. B* **37**, 1884 (1988).
- [24] A. Ortega, T. Stegmann, and L. Benet, *Phys. Rev. E* **98**, 012141 (2018).
- [25] S. John, *Phys. Rev. Lett.* **53**, 2169 (1984).
- [26] P. W. Anderson, *Philos. Mag. B*, **52**, 505 (1985).
- [27] E. Akkermans, P. E. Wolf, R. Maynard, and G. Maret, *J. Phys. France* **49**, 77 (1988).
- [28] Y. Lahini, A. Avidan, F. Pozzi, M. Sorel, R. Morandotti, D. N. Christodoulides, and Y. Silberberg, *Phys. Rev. Lett.* **100**, 013906 (2008).
- [29] The collective shift and decay rate are given by the real and imaginary parts of the Green function connecting the free field that propagates between two atoms,
- $$\Delta_{ss'}^{nm} + i\frac{1}{2}\gamma_{ss'}^{nm} = \frac{3\pi\Gamma_0}{k_0} \mathbf{e}_s^* \cdot \mathbf{G}(z_n - z_m, \omega_0) \cdot \mathbf{e}_s,$$
- where  $\hat{\epsilon}_s$  are unitary operators along the  $s$  direction,  $k_0 = \omega_0/c$ , and the propagator takes the explicit form,
- $$\mathbf{G}(\mathbf{r}, \omega_0) = \frac{k_0}{4\pi} \frac{e^{i\xi}}{\xi^3} \left[ (\xi^2 + i\xi - 1)\mathbb{1} - (\xi^2 + 3i\xi - 3) \frac{\mathbf{r} \otimes \mathbf{r}}{r^2} \right],$$
- with  $\xi = k_0 r$ .
- [30] G. L. Celardo and L. Kaplan, *Phys. Rev. B* **79**, 155108 (2009).
- [31] G. L. Celardo, A. M. Smith, S. Sorathia, V. G. Zelevinsky, R. A. Sen'kov, and L. Kaplan, *Phys. Rev. B* **82**, 165437 (2010).
- [32] T. S. Tsoi and C. K. Law, *Phys. Rev. A* **78**, 063832 (2008).
- [33] A. Asenjo-Garcia, J. D. Hood, D. E. Chang, and H. J. Kimble, *Phys. Rev. A* **95**, 033818 (2017).
- [34] D. F. Kornovan, M. I. Petrov, and I. V. Iorsh, *Phys. Rev. B* **96**, 115162 (2017).
- [35] D. Mukhopadhyay and G. S. Agarwal, *Phys. Rev. A* **100**, 013812 (2019).
- [36] H. J. Carmichael and K. Kim, *Opt. Commun.* **179**, 417 (1999).
- [37] C. Cohen-Tannoudji, J. Dupont-Roc, and G. Grynberg, *Atom-Photon Interactions: Basic Processes and Applications*, Complement BIII (Wiley, Hoboken, 1989).
- [38] H. J. Carmichael, in *Statistical Methods in Quantum Optics 1*, (Springer-Verlag, Berlin/Heidelberg, 1999), Chap. 2.
- [39] C. Gardiner and P. Zoller, in *Quantum Noise* (Springer-Verlag, Berlin/Heidelberg, 1991, 2000), Chap. 3.
- [40] U. Fano, *Phys. Rev.* **124**, 1866 (1961).
- [41] P. A. Mello, *Phys. Lett. B* **81**, 103 (1979).
- [42] V. V. Sokolov and V. G. Zelevinsky, *Ann. Phys. (NY)* **216**, 323 (1992).
- [43] F.-M. Dittes, *Phys. Rep.* **339**, 215 (2000).
- [44] Y. Hadad, Y. Mazor, and Ben Z. Steinberg, *Phys. Rev. B* **87**, 035130 (2013).
- [45] Y. Mazor, Y. Hadad, and Ben Z. Steinberg, *Phys. Rev. B* **92**, 125129 (2015).
- [46] R. Landauer, *Z. Phys. B: Condens. Matter* **68**, 217 (1987).